Liu, Z.T.Y., Burton, B.P., Khare, S.V., Sarin, P., 2016. Chemical Geology 443, 137-145 (2016)

First-principles phase diagram calculations for the carbonate quasi-binary systems $CaCO_3$-$ZnCO_3$, $CdCO_3$-$ZnCO_3$, $CaCO_3$-$CdCO_3$ and $MgCO_3$-$ZnCO_3$

Z. T. Y. Liu[a], B. P. Burton[b], S. V. Khare[a*], P. Sarin[c]

[a]Department of Physics and Astronomy, University of Toledo, Toledo, OH 43606, USA

[b]Materials Measurement Laboratory, Metallurgy Division, National Institute of Standards and Technology (NIST), Gaithersburg, MD 20899, USA

[c]School of Materials Science and Engineering, Oklahoma State University, Tulsa, OK 74106, USA

Correspondence author: sanjay.khare@utoledo.edu

Supplementary Material

Table S1 Structural parameters of the calcite ($CaCO_3$) prototype used in the calculations. The other structures can be obtained through substitution and relaxation.

	x (Å)	y (Å)	z (Å)
a	4.640	-0.008	4.480
b	1.897	4.235	4.480
c	-0.012	-0.008	6.450
	u_1	u_2	u_3
Ca	0.500	0.500	0.500
Ca	0.000	0.000	0.000
C	0.750	0.750	0.750
C	0.250	0.250	0.250
O	0.750	0.493	0.007
O	0.007	0.750	0.493
O	0.507	0.993	0.250
O	0.250	0.507	0.993
O	0.993	0.250	0.507
O	0.493	0.007	0.750

A. Cluster expansion formalism

In the brief description given below we provide a theoretical formalism, developed in the literature (Connolly and Williams, 1983; De Fontaine, 1994; Ducastelle, 1991; Laks et al., 1992; Sanchez et al., 1984; Zunger, 1994) over the last three decades, that allows the computation of binary and higher-order temperature-composition phase diagrams purely from first-principles calculations.

The MIT Ab-initio Phase Stability (maps) (van de Walle, 2009; van de Walle et al., 2002) code in ATAT reads in the provided lattice and automatically generates structures with different compositions at the chemically exchangeable sites. It further calculates the total energy with density functional theory (DFT) through cell volume, shape and atom position optimization and fits resulting DFT energy values to a compact polynomial representation, i.e. cluster expansion (CE),

$$E(\sigma) = \sum_\alpha m_\alpha J_\alpha \langle \prod_{i\in\alpha} \sigma_i \rangle_\alpha. \qquad \text{(Eqn. 1)}$$

In this formula, α is a cluster of a set of exchangeable sites (i) in the parent lattice, and each exchangeable site is assigned a configuration variable σ_i. In a binary $M^A_{1-x}M^B_x$, or quasibinary, e.g. $M^A_{1-x}M^B_xCO_3$, σ_i takes values -1 and +1 respectively. The sum is taken over all the symmetrically inequivalent clusters of the parent lattice, and the average, denoted by angular brackets, is over all clusters symmetrically equivalent to α, m_α being its multiplicity. Coefficients J_α are called effective cluster interactions (ECIs).

The optimal cluster set and its ECIs are selected by minimizing the cross-validation (CV) score,

$$CV = \frac{1}{n}\sum_{i=1}^{n}\left(E_i - \hat{E}_{(i)}\right)^2, \qquad \text{(Eqn. 2)}$$

where E_i is the *ab initio* calculated energy of structure *i*, and $\hat{E}_{(i)}$ is the "leave-one-out" (without structure *i*) least-squares fitted energy to prevent over-fitting. This process is carried out iteratively when the *ab*

initio energy of a new structure is included. As the structure set grows, the cluster set typically grows as well to enhance the predictive power of the CE.

Table S2 Cluster sets and effective cluster interactions (ECIs) of the $Ca_{1-x}Zn_xCO_3$, $Cd_{1-x}Zn_xCO_3$, $Ca_{1-x}Cd_xCO_3$ and $Mg_{1-x}Zn_xCO_3$ systems.

Type	Index	Diameter (Å)	Multiplicity	Coordinates	ECI [$Ca_{1-x}Zn_xCO_3$] (meV)	ECI [$Cd_{1-x}Zn_xCO_3$] (meV)	ECI [$Ca_{1-x}Cd_xCO_3$] (meV)	ECI [$Mg_{1-x}Zn_xCO_3$] (meV)
empty	1	0.000	1		149.872	104.469	1.246	-1.745
point	1	0.000	2	[[0.5, 0.5, 0.5]]	6.986	5.571	-0.220	-0.002
pair	1	4.097	6	[[0.5, 0.5, 0.5], [1.0, -0.0, 1.0]]	7.762	4.001	1.043	0.900
pair	2	5.052	6	[[1.0, 1.0, 1.0], [1.0, 2.0, 0.0]]	-15.694	-10.951	-1.293	-0.209
pair	3	6.450	6	[[0.5, 0.5, 0.5], [0.5, 0.5, -0.5]]	-2.172	-1.966	0.246	-0.297
pair	4	6.505	6	[[1.0, 1.0, 1.0], [1.5, 1.5, -0.5]]	6.381	5.974	-0.900	-0.003
pair	5	8.193	6	[[0.5, 0.5, 0.5], [-0.5, 1.5, -0.5]]	-1.832	-1.856		-0.078
pair	6	8.236	12	[[0.5, 0.5, 0.5], [-0.0, 2.0, -1.0]]	-4.403	-2.833		
pair	7	8.629	2	[[0.5, 0.5, 0.5], [0.0, 0.0, 0.0]]	-3.071	-1.640		
pair	8	8.751	6	[[1.0, 1.0, 1.0], [-0.0, 3.0, 0.0]]	-1.644	-1.285		
pair	9	9.626	6	[[1.0, 1.0, 1.0], [1.0, 2.0, -1.0]]	2.370	1.565		
pair	10	9.626	6	[[0.5, 0.5, 0.5], [0.5, 1.5, -1.5]]	0.000	0.000		
pair	11	9.999	12	[[0.5, 0.5, 0.5], [-0.0, 1.0, -1.0]]	-1.452	-1.273		
pair	12	10.105	6	[[1.0, 1.0, 1.0], [1.0, 3.0, -1.0]]	0.126	0.365		
pair	13	10.904	12	[[0.5, 0.5, 0.5], [1.0, 2.0, -2.0]]	-1.108	-0.599		
pair	14	11.869	6	[[1.0, 1.0, 1.0], [1.0, 2.0, 2.0]]	-1.756	-1.089		

pair	15	11.988	6	[[1.0, 1.0, 1.0], [-0.0, 3.0, -1.0]]	-3.290	-2.207	
pair	16	11.988	6	[[0.5, 0.5, 0.5], [-0.5, 2.5, -1.5]]	0.000	0.000	
trip	1	5.052	12	[[1.0, 1.0, 1.0], [0.5, 1.5, 0.5], [1.0, 2.0, 0.0]]	0.473	0.695	0.062
trip	2	5.052	4	[[1.0, 1.0, 1.0], [-0.0, 2.0, 1.0], [1.0, 2.0, 0.0]]	-0.207	0.240	0.000
trip	3	6.450	12	[[0.5, 0.5, 0.5], [-0.0, 1.0, -0.0], [0.5, 0.5, -0.5]]	0.624	0.237	-0.052
trip	4	6.450	12	[[0.5, 0.5, 0.5], [0.5, 1.5, -0.5], [0.5, 0.5, -0.5]]	-0.485	-0.132	0.012
trip	5	6.505	12	[[1.0, 1.0, 1.0], [0.5, 1.5, 0.5], [1.5, 1.5, -0.5]]	-1.728	-1.359	
trip	6	6.505	12	[[1.0, 1.0, 1.0], [1.5, 0.5, 0.5], [1.5, 1.5, -0.5]]	0.000	0.000	
trip	7	6.505	12	[[1.0, 1.0, 1.0], [1.5, 1.5, 0.5], [1.5, 1.5, -0.5]]	0.717	0.249	
trip	8	8.193	6	[[0.5, 0.5, 0.5], [-0.0, 1.0, -0.0], [-0.5, 1.5, -0.5]]	-3.374	-1.169	
trip	9	8.193	12	[[0.5, 0.5, 0.5], [0.5, 1.5, -0.5], [-0.5, 1.5, -0.5]]	0.668	-0.161	
trip	10	8.193	12	[[0.5, 0.5, 0.5], [-0.5, 1.5, 0.5], [-0.5, 1.5, -0.5]]	0.000	0.000	

trip	11	8.193	12	[[0.5, 0.5, 0.5], [1.0, 1.0, -1.0], [-0.5, 1.5, -0.5]]	0.266	0.046	
quad	1	5.052	4	[[1.0, 1.0, 1.0], [0.5, 1.5, 0.5], [-0.0, 2.0, 1.0], [1.0, 2.0, 0.0]]			0.996

B. Vibrational contributions

Vibrational free energy contributions to the phase diagrams were added through the stiffness vs length transferable force constants method (fitsvsl and svsl code in ATAT) (van de Walle and Ceder, 2002; van de Walle, 2013, 2009). It is based on the observation that bond length is typically a good predictor of bond stiffness for a given lattice and given type of bond. This approach is advantageous over the direct calculation of phonon contributions of all structures in a set because only a few structures are needed to derive the stiffness vs. length relationship. Then this relationship is used to get the (a) force constants, (b) dynamical matrices, (c) phonon spectra and (d) vibrational free energies for all structures in the CE set. Quasi-harmonic approximation considering volume expansion was used. In our calculations, we selected 10 structures to extract the information on the force constants. The minimum distance between displaced atoms was set to 9 Å, displacement of the perturbed atom to 0.2 Å, strain of the maximum volume sampled to 0.01 with 3 volume sampling points and a linear fit was performed.

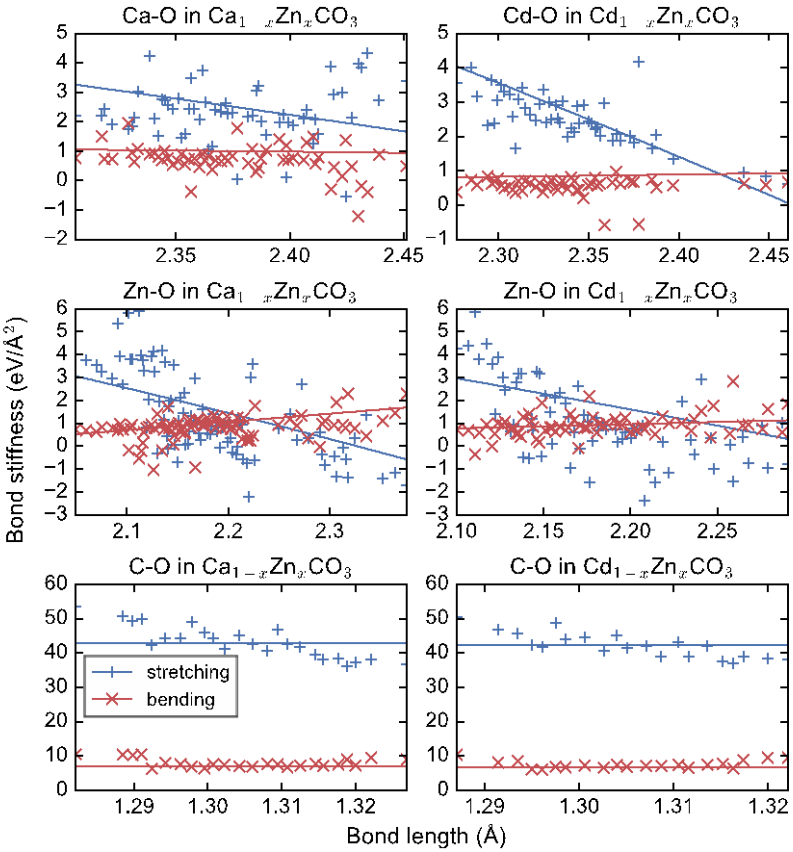

Figure S1 Nearest neighbor stretching and bending stiffness constants versus bond lengths of various bonds in $Ca_{1-x}Zn_xCO_3$ and $Cd_{1-x}Zn_xCO_3$. Blue "+" and red "×" crosses stand for stretching and bending terms respectively. Lines are linear fits, which were used in the calculations of vibrational free energy contributions.

We included vibrational free energy contributions for $Ca_{1-x}Zn_xCO_3$ and $Cd_{1-x}Zn_xCO_3$, because the consolute temperature is above 1000 K, so they are likely to be significant. Figure S1 illustrates the bond stiffness vs bond length relations and the linear fits thereto. The C-O bonds in both systems are the most rigid and exhibit little scatter, but Ca-O, Cd-O and Zn-O bonds exhibit noticeable scatter. These bond stiffness values are an order of magnitude smaller than those of C-O, so they contribute to softer modes of vibration.

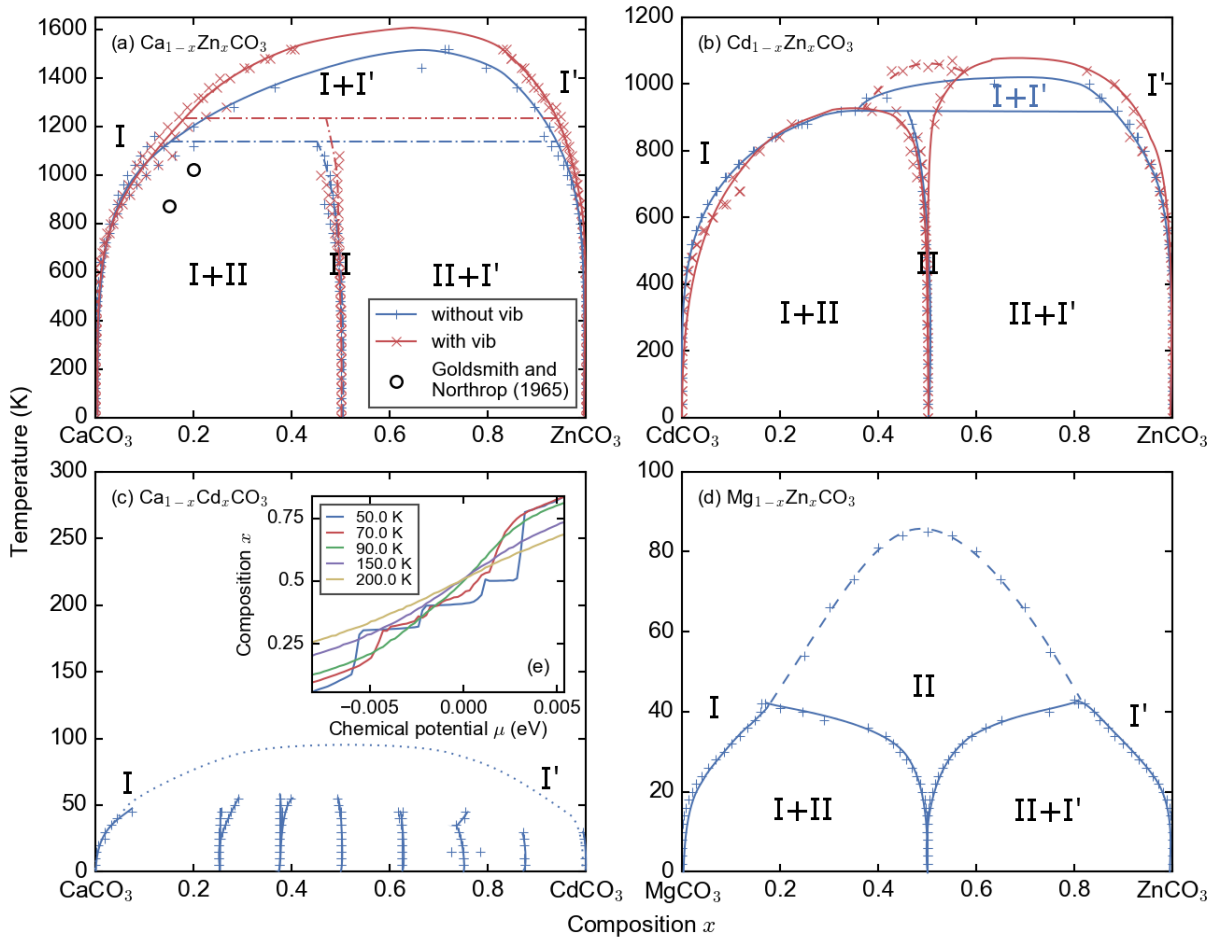

Figure S2 Calculated phase diagrams of (a) $Ca_{1-x}Zn_xCO_3$, (b) $Cd_{1-x}Zn_xCO_3$, (c) $Ca_{1-x}Cd_xCO_3$ and (d) $Mg_{1-x}Zn_xCO_3$. Crosses are the raw data points, and curves are interpolations and extrapolations. In (a), blue "+" and red "×" solid curves correspond to results without and with vibrational contributions, respectively. Dash-dotted curves stand for influence of the dolomite structure on the topology of the phase diagrams. Hollow circles are experimental data points. In (b), the dashed curve stands for the continuous order-disorder transition points. In (c), the dotted curve stands for the estimated consolute boundary, as demonstrated by the inset (e). In (d), the dashed curve has the same meaning as in (b). In all 4 subfigures, calcite-structure phases are labeled as I and I', and dolomite-structure phases as II. In (e), curves stand for compositions with respect to chemical potentials at various temperatures in a semi-grand-canonical ensemble simulation.

The phase diagrams are shown in Figure S2. The relevant temperatures are summarized in Table S3. For $Ca_{1-x}Zn_xCO_3$ in Figure S2(a), vibrational contributions lead to an increase in consolute temperature from 1450 K to 1600 K. The peritectoid point of the dolomite-structure phase increases from 1150 K to 1250 K. For $Cd_{1-x}Zn_xCO_3$ in Figure S2(b), the dolomite-structure phase splits through the miscibility gap between the end members, and the peritectoid point at 900 K becomes an order-disorder transition line, reaching maximum at 1050 K. Figure S3 shows the abrupt drops of the long-range order in these two systems. We conclude that the vibrational free energy contributes to the dolomite-structure phase favorably and renders it with better stability, delaying its order-disorder transition.

Table S3 Consolute temperatures (T_C), peritectoid points (T_P) and dolomite order-disorder transition temperatures (T_{trans}) of $Ca_{1-x}Zn_xCO_3$, $Cd_{1-x}Zn_xCO_3$, $Ca_{1-x}Cd_xCO_3$ and $Mg_{1-x}Zn_xCO_3$. Vibrational free energy contributions are shortened as "vib".

	T_C without vib (K)	T_C with vib (K)	T_P without vib (K)	T_P with vib (K)	T_{trans} without vib (K)	T_{trans} with vib (K)

$Ca_{1-x}Zn_xCO_3$	1450	1600	1150	1250		
$Cd_{1-x}Zn_xCO_3$	1000		900			1050
$Ca_{1-x}Cd_xCO_3$	< 100					
$Mg_{1-x}Zn_xCO_3$					< 100	

It is worth pointing out that because of the scatter of the bond stiffness vs bond length relations for the softer M-O bonds in Figure S1, and the closeness to 0 of dolomite structures' ΔE_f, error might have influenced the evaluation of the peritectoid point in $Cd_{1-x}Zn_xCO_3$. We did several trials with increasing numbers of structures to extract the information on the force constants, and large variations (200 K) occurred to the resultant consolute and transition temperatures. A high quality yet low-cost approach needs to be developed to further address this problem.

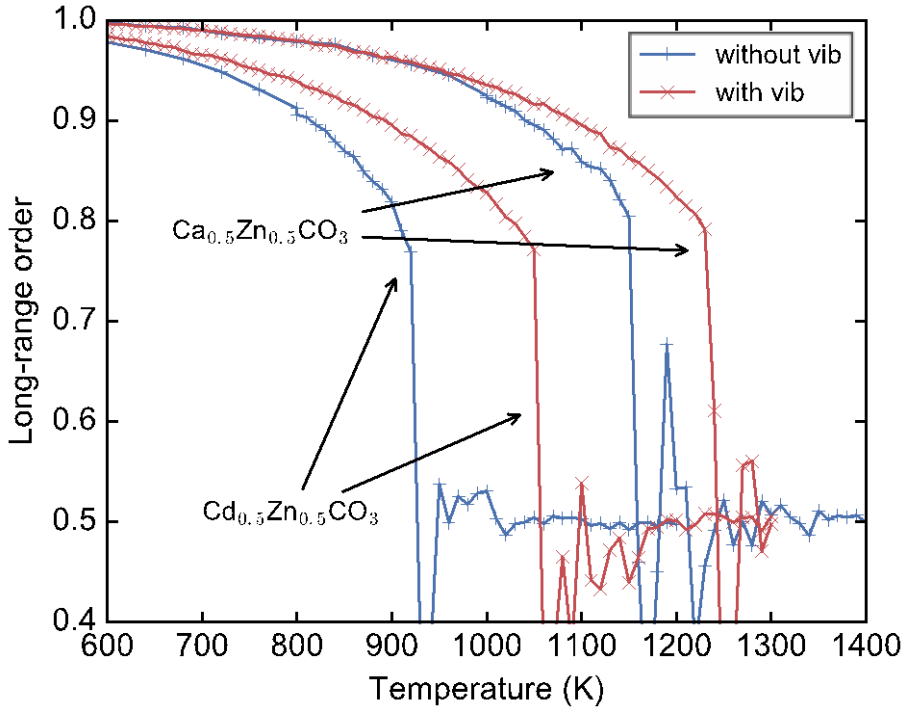

Figure S3 Long-range order as a function of temperature for $Ca_{0.5}Zn_{0.5}CO_3$ and $Cd_{0.5}Zn_{0.5}CO_3$ in canonical ensemble simulations. Blue "+" and red "×" curves correspond to results without and with the vibrational contributions, respectively. The onsets of the abrupt drops to 0.5 mark the transition temperatures of the dolomite-structure phases.

References

Connolly, J.W.D., Williams, A.R., 1983. Density-Functional Theory Applied to Phase-Transformations in Transition-Metal Alloys. Phys. Rev. B 27, 5169–5172. doi:10.1103/PhysRevB.27.5169

De Fontaine, D., 1994. Cluster approach to order-disorder transformations in alloys. Solid State Phys. - Adv. Res. Appl. Vol 47 47, 33–176.

Ducastelle, F., 1991. Order and Phase Stability in Alloys. Elsevier Science, New York.

Laks, D.B., Ferreira, L.G., Froyen, S., Zunger, A., 1992. Efficient Cluster-Expansion for Substitutional Systems. Phys. Rev. B 46, 12587–12605. doi:10.1103/PhysRevB.46.12587

Sanchez, J.M., Ducastelle, F., Gratias, D., 1984. Generalized Cluster Description of Multicomponent

Systems. Physica A 128, 334–350. doi:10.1016/0378-4371(84)90096-7
van de Walle, A., 2013. Methods for First-Principles Alloy Thermodynamics. JOM J. Miner. Met. Mater. Soc. 65, 1523–1532. doi:10.1007/S11837-013-0764-3
van de Walle, A., 2009. Multicomponent multisublattice alloys, nonconfigurational entropy and other additions to the Alloy Theoretic Automated Toolkit. Calphad-Computer Coupling Phase Diagrams Thermochem. 33, 266–278. doi:10.1016/J.Calphad.2008.12.005
van de Walle, A., Asta, M., Ceder, G., 2002. The Alloy Theoretic Automated Toolkit: A user guide. Calphad-Computer Coupling Phase Diagrams Thermochem. 26, 539–553. doi:10.1016/S0364-5916(02)80006-2
van de Walle, A., Ceder, G., 2002. The effect of lattice vibrations on substitutional alloy thermodynamics. Rev. Mod. Phys. 74, 11–45. doi:10.1103/Revmodphys.74.11
Zunger, A., 1994. First principles statistical mechanics of semiconductor alloys and intermetallic compounds, in: Turchi, P.E., Gonis, A. (Eds.), NATO ASI on Statics and Dynamics of Alloy Phase Transformation. Plenum Press, New York, p. 361.